Flowing afterglow system for surface treatment of heat sensitive small diameter tubes

Kinga Kutasi § and Ihor Korolov

Wigner Research Centre for Physics, Research Institute for Solid State Physics and Optics, Hungarian Academy of Sciences, POB 49, H-1525 Budapest, Hungary

Abstract.

The flowing afterglow of an N_2-O_2 surface-wave microwave discharge is used to demonstrate the possibility of treating simultaneously the inner and outer surfaces of heat sensitive small diameter tubes in low pressure afterglows. It is shown that the afterglow can be efficiently guided through a 4.5 mm polymer tube, as well as similar afterglows can flow simultaneously inside and around the tube at gas flow rates in the range of 500-1000 sccm. A 5 mm inner diameter quartz tube is used to study the afterglow guided through small diameter tubes, by following the evolution of the UV emission originating from the excited NO molecules created in the three-body re-association process of N and O-atoms. The afterglows in the reactor and in the quartz tube are characterized using a 3-D hydrodynamic model. According to the calculated density distributions the relative density of atoms do not change considerably along the tube placed into reactor. The calculated gas temperature distribution in the reactor shows that the position of the heat sensitive tube in the reactor should be carefully chosen, e.g. in the second half of a 4.4 cm diameter and 40 cm long reactor.

§ e-mail: kutasi.kinga@wigner.mta.hu

1. Introduction

The treatment and modification of surfaces by reactive plasmas is a widespread method. Reactive oxygen and UV radiating plasmas have been suggested for sterilization and decontamination of surfaces [1, 2, 3, 4, 5, 6, 7], etching and grafting of polymers [8, 9, 10, 11, 12, 13, 14], as well as for functionalization, structuring and activation of surfaces [15, 16, 17, 18, 19]. One of the main targets are the polymers, which find their use in biomedicine [20, 21, 22, 23]. For treatment of heat sensitive polymers low temperature environment is required, which can be easily achieved in afterglow plasmas. The afterglow of a low pressure flowing surface-wave microwave discharge has been found a proper medium [1, 2, 7, 9, 13, 14, 17, 24, 25], since it can be easily tuned to achieve high density of active species at low gas temperature [13, 26, 27, 28, 29, 30, 31]. Although this system has been tested for several applications, the efficient treatment of objects with complex geometry is still an open question. The aim of the present work is to determine the possibility of treating simultaneously the inner and outer surfaces of small diameter tubes in the afterglow of a low pressure surface-wave microwave discharge.

The treatment of the inner surface of small diameter tubes by plasmas has been realized under discharge conditions, both at low and atmospheric pressures. At low pressure the discharge has been ignited with a low or high-frequency field inside the tube using different discharge system configurations [32, 33, 34, 35, 36, 38] . At atmospheric pressure the transfer of the atmospheric-pressure plasma into a tube has been realized by producing an ionization wave (IW) in a tube or channel by impingement of a separately produced IW onto its outer surface [39]. Discharges have also been ignited directly into small diameter tubes, e.g. a pulsed corona discharge was ignited into an 8 mm ID quartz tube using gas flow rates in the 4-5 slm range and by placing the electrodes at the two ends of the tube [37]. The simultaneous treatment of the inner and outer wall of a tube has been recently realized under discharge condition at atmospheric pressure by treating the outer wall by an Ar (2 slm) plasma jet and meanwhile inducing transferred He (3 slm) plasma inside the perpendicularly positioned 2 mm ID PTFE tube [40]. The overall treatment of the outer wall of the tube is realized by its continuous turning. Under discharge conditions the surface is exposed both to neutral and energetic charged species, which may induce a stronger surface modification, i.e. a more efficient etching of the surface, while the surface temperature can increase above the 40°C required by the heat sensitive polymers. In our work we propose a milder surface modification - as also illustrated in ref. [41] on Polystyrene microspheres treated for hours in a similar late-afterglow -, which relies only on neutral species and targets the surface oxidation processes [1].

Our investigations are carried out in the afterglow of a low pressure N_2-O_2 surface-wave microwave discharge sustained with an input power of 25 W using gas flow rates in the range of 0.5-1 slm. We note that the afterglow plasma has been already tested for the treatment of the inner wall of an 8 mm ID quartz tube at atmospheric pressure by using the afterglow of an N_2-O_2 atmospheric pressure corona discharge [42]. In this case

the gas flow rates of 40 slm were used. The low pressure afterglow system used in our studies and the experimental methods are presented in Section 2. The N_2-O_2 mixture is chosen due to its strong UV radiation originating from the excited NO molecules, which offers a good diagnostic tool [26], and the visible radiation, which makes possible to visualize the transport of the afterglow through and around the treated tube. The afterglow system is characterized by means of modelling, as presented in Section 3. The different treatment possibilities and the system characteristics are presented in Section 4.

2. Afterglow system configuration and experimental methods

The afterglow system proposed for the surface treatment of small diameter tubes is based on a surface-wave microwave discharge generated with the help of a surfatron in flowing gas. In the system here investigated - presented in Figure 1 - the discharge tube is a 5 mm ID and 50 cm long quartz tube (QT1). The discharge tube is connected to a 44 mm ID reactor tube (QT2), where the active species from the discharge are transported. The gas flow is ensured by two rotary pumps of 25 m^3h^{-1} nominal speed connected in parallel. The different gases are introduced into the system through flow controllers. The pressure is measured at the gas inlet and downstream of the reactor.

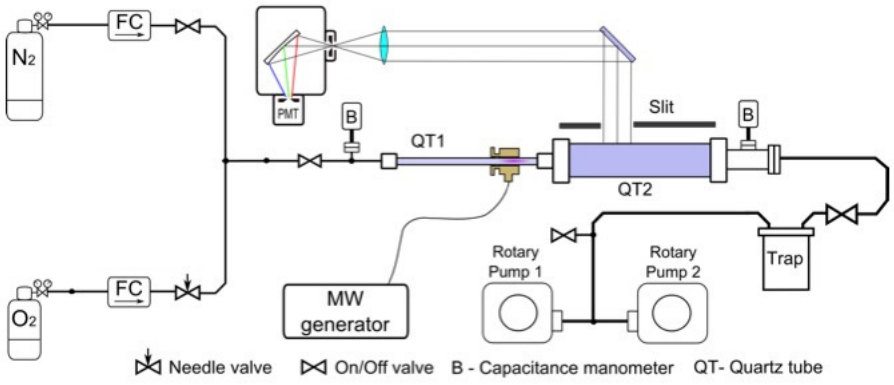

Figure 1. The scheme of the experimental system with QT1 marking the discharge tube and QT2 the afterglow tube.

Figure 2. The image of the afterglow system set-up with the small diameter tube placed into reactor.

The small diameter tube to be treated is placed into the afterglow reactor and held by two identical teflon rings in the middle axis of the reactor, as shown in Figure 2.

Teflon is chosen due to its heat resistance and the low recombination probability of atoms on its surface [43]. In the treatment process two important situations need to be distinguished - i.e. treatment of (*i*) the inner wall of the tube and (*ii*) both the inner and outer walls -, which require two different types of tube holders. In the first case, when the treatment of the tube's inner wall is targeted, the tube should be perfectly fitted in the middle of a solid teflon ring, which has the same diameter as the reactor. In this way the afterglow species can be transported through the treated tube. In the second case, in order to achieve similar afterglow both inside and outside the treated tube, on the teflon ring symmetrically positioned holes are drilled, whose capacitance should be equal to that of the tube's.

The discharge is ignited in N_2-O_2 mixture at 25 W using gas flow rates in the 500-1000 sccm range. The pressure in the system, as discussed later in Section 4.3.1 will vary based on the loading of the reactor. At these conditions, as indicated also by the emission spectra presented in Section 4.3.1, in the reactor a neutral late-afterglow plasma will be present [1, 26, 31].

The evolution of the afterglow in the reactor and in the treated tube is experimentally followed and visualized through the optical emission. In an N_2-O_2 late-afterglow the strongest (non-resonant) emission which is directly correlated to the density of active atoms, i.e. O-atoms and N-atoms, originates from the excited NO molecules [26] and occurs in the UV region in the 200 - 350 nm spectral range. The emission spectra recorded in this region can give information on the presence of the atoms, which participate in the surface treatment processes. The UV emission is very strong at low O_2 content mixtures, while in the case of mixtures with O_2>10% the emission in the visible range (yellow-green) originating from the NO_2 molecules becomes dominant [44]. The light is collected from a 0.5 cm width segment at the axis of the reactor and focused into an Acton VM-502 monochromator (20 cm focal length, 1200 grooves/mm grating providing a resolution of 0.08 nm at a slit width of 20 μm) equipped with a Hamamatsu (H7732P-11) photomultiplier tube whose signal is recorded in photon counting mode.

3. Modelling technique

In order to understand better the afterglow system under different loading conditions and to define its application limits we choose the modelling technique. The validity of the modelling scheme used has been presented in several previous publications [26, 45, 31, 49]

The evolution of the afterglow in the reactor and in the tube placed in the reactor is followed with a three-dimensional hydrodynamic model, which allows the determination of the gas velocity field, the species densities and the gas temperature distributions. The three-dimensional hydrodynamic model [50, 51] is composed of (i) the total mass conservation, (ii) the continuity equations for the different species, (iii) the

total momentum conservation equation, and (iv) the total energy conservation equation:

$$\int_S \rho \mathbf{v} \cdot \mathbf{n}\, dS = 0\ , \tag{1}$$

$$\int_S \rho y_k \mathbf{v} \cdot \mathbf{n}\, dS - \int_S \nabla(D_k \rho\, y_k) \cdot \mathbf{n}\, dS = \int_V m_k\, S_k^{\mathrm{V}}\, dV + \int_S m_k\, S_k^{\mathrm{S}}\, dS\ , \tag{2}$$

$$\int_S \rho u_i \mathbf{v} \cdot \mathbf{n}\, dS = \int_S \mu\ grad\ u_i \cdot \mathbf{n}\, dS - \int_S p \mathbf{i}_i \cdot \mathbf{n}\, dS\ , \tag{3}$$

$$\int_S \rho T \mathbf{v} \cdot \mathbf{n}\, dS = \int_S \frac{\lambda}{C_p}\ grad\, T \cdot \mathbf{n}\, dS\ . \tag{4}$$

Here ρ denotes the total gas density, $\mathbf{v}$ the gas velocity and $\mathbf{n}$ the unit vector orthogonal to the S surface and directed outwards. Further, y_k denotes the relative mass density (y_k=ρ_k/ρ), D_k and m_k are the diffusion coefficient and the mass of the species k, and S_k^{V} and S_k^{S} represent the source terms associated with volume and surface reactions, respectively. u_{i} is the velocity in the i direction, p the static pressure, μ the dynamic viscosity, T is the gas temperature, C_p the specific heat at constant pressure and λ the thermal conductivity. For more details readers can refer to ref. [48].

The gas phase reaction kinetic scheme used in the hydrodynamic model, which takes into account only the neutral species, has been presented in [26, 47, 50] together with the reaction rates used, while the surface processes have been discussed in details in [51], and in the present case we choose the surface recombination probabilities valid for glass surfaces.

The relative density of species entering the reactor, which serve as an initial condition for the hydrodynamic model, are determined with the kinetic model for the discharge and early-afterglow regions, described in details in ref. [45, 46], which uses the reaction kinetic scheme presented in ref. [47]. The discharge model is based on the stationary homogeneous electron Boltzmann equation solved for the microwave field, using the effective field approximation, coupled to a system of rate-balance equations for the neutral and charged heavy species: $N_2(X^1\Sigma_g^+,\ v)$, $O_2(X^3\Sigma_g^-,\ v')$, $N_2(A^3\Sigma_u^+$, $B^3\Pi_g$, $B'^3\Sigma_u^-$, $C^3\Pi_u$, $a'^1\Sigma_u^-$, $a^1\Pi_g$, $w^1\Delta_u)$, $O_2(a^1\Delta_g)$, $O_2(b^1\Sigma_g^+)$, $N(^4S)$, $O(^3P)$, $N(^2D$, $^2P)$, $NO(X^2\Pi)$, $NO(A^2\Sigma^+)$, $NO(B^2\Pi)$, NO_2(X,A), O_3, $N_2^+(X^2\Sigma_g^+$, $B^2\Sigma_u^+)$, N_4^+, O_2^+, O^+, NO^+ and O^-. The early-afterglow, which develops downstream of the discharge in the same tube, is described with the same rate-balance equations (neglecting the electron impact excitation/ionization processes), whose time-dependent solutions constitute the initial conditions for the hydrodynamic model.

4. Results and Discussion

4.1. Guiding the afterglow through the small diameter tube

In order to guide the afterglow through a small diameter tube, the tube is placed into the reactor with the help of two teflon rings, as described in Section 2. The applicability

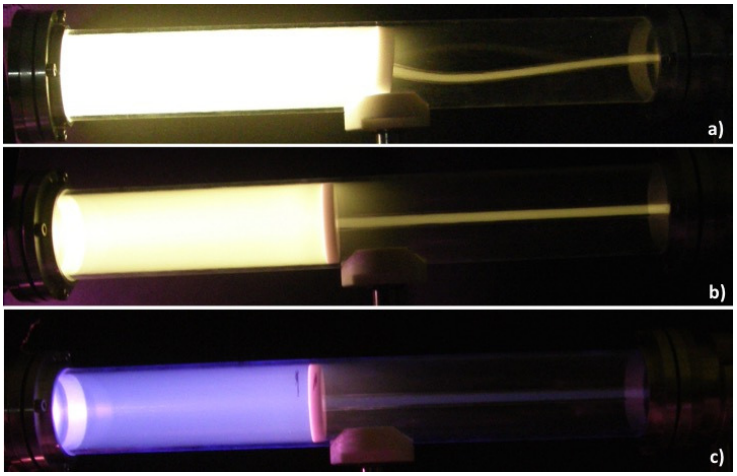

Figure 3. The image of the afterglow reactor loaded with: (a) a polymer tube in the case of a 300 sccm Ar - 100 sccm N_2 - 100 sccm O_2 mixture discharge, and with a quartz tube in the case of discharges ignited at (b) 400 sccm N_2 - 100 sccm O_2 and (c) 1000 sccm N_2 - 20 sccm O_2 flow conditions.

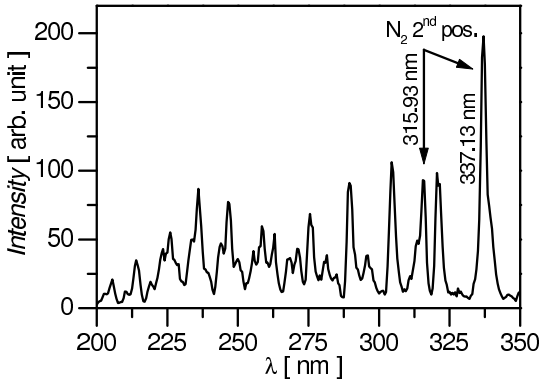

Figure 4. The spectra measured at the middle position of the 5 mm diameter quartz tube in the case of a 1000 sccm N_2 - 20 sccm O_2 mixture discharge.

of the system for the surface treatment of heat sensitive tubes is demonstrated by using a 20 cm long flexible polymer tube of 4.5 mm inner diameter. Afterwards, in order to be able to follow the UV emitting species - and indirectly the active atoms - along the system through the optical emission spectra, the polymer tube is replaced with a quartz tube of 5 mm inner diameter. Figure 3 shows the images taken from the afterglow reactor loaded with the different tubes in the case of discharges with different flow conditions and mixture compositions. The images clearly show the transport of the afterglow through the tube in the case of 500 - 1000 sccm gas flow rates. The images illustrate that - as already stated - in the case of high O_2 content mixtures the afterglow is dominated by the yellow-green emission originating predominantly from the NO_2 molecules, while at low, such as 2%O_2 the UV emission dominates. Figure 4 shows the spectra measured (as illustrated in Figure 1) at the middle position of the quartz

tube for the 1000 sccm N_2 - 20 sccm O_2 flow condition. In the spectra emission of the NO_γ, NO_β and N_2 second positive system are identified. We note, that at low O_2 flows the flow controller becomes unstable, therefore the O_2 content of the mixture can fluctuate during the measurements, which results in the variation (decrease) of the NO_γ and NO_β intensities.

4.2. Afterglow flowing simultaneously inside and around the small diameter tube

In order to make possible the simultaneous treatment of the inner and outer walls of the tube, similar afterglow should flow both inside and around the tube. To realize this, the 5 mm ID and 20 cm long quartz tube is held in the reactor by two 5 mm thick teflon rings with four pair of 2 mm holes symmetrically positioned around the tube's position. Figure 5 shows the image of the reactor loaded with the tube for two different flow conditions. In order to make visible the flow of the afterglow inside the tube, a stainless steel surface is placed in the reactor around the quartz tube to enhance the recombination of the active atoms outside the tube (in case of stainless steel the surface recombination probability of atoms is in the range of 10^{-2}) [51] . As a consequence, due to the decrease of the density of atoms the densities of excited NO and NO_2 molecules and the corresponding light emission diminish.

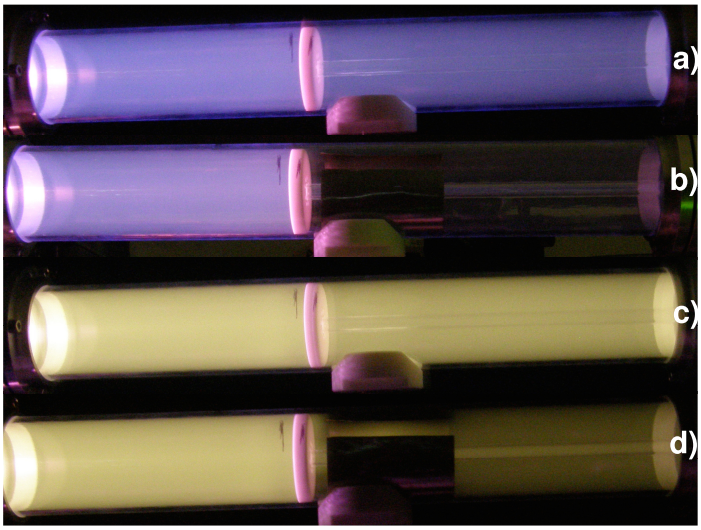

Figure 5. The image of the afterglow reactor loaded with the 5 mm ID quartz tube at (a)-(b) 1000 sccm N_2 - 20 sccm O_2 and (c)-(d) 1000 sccm N_2 - 100 sccm O_2 flow conditions. The tube is held by a teflon ring with 2 mm holes symmetrically positioned around the tube's position. In the (b) and (d) cases a stainless steel surface is placed around the quartz tube to eliminate the N and O-atoms, and as a consequence, the excited NO and NO_2 molecules.

Figure 6 shows the spectra measured in the loaded part of the reactor in the flow axis at 4 cm from the tube's left end in the case of 1000 sccm N_2 - 20 sccm O_2 flow. In this case the light is collected both from inside and outside the tube placed into reactor.

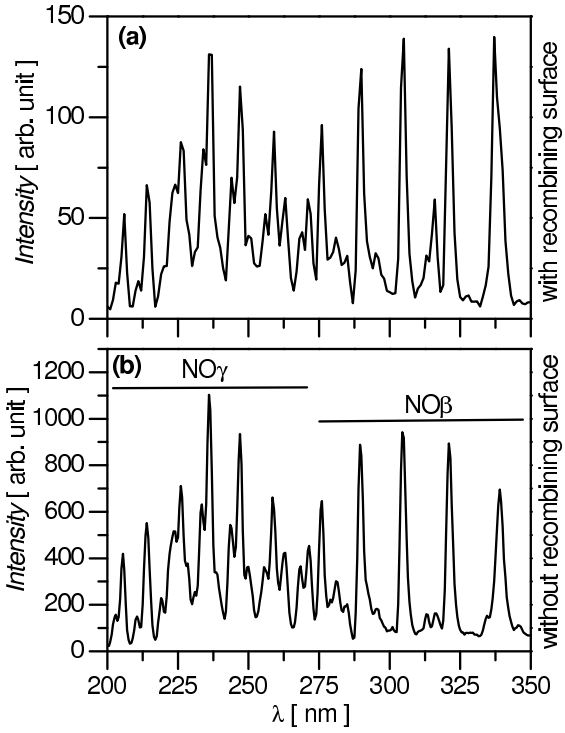

Figure 6. The spectra in the loaded part of the reactor at 4 cm from the quartz tube's left end for the 1000 sccm N_2 - 20 sccm O_2 flow condition (a) with and (b) without the presence of the recombining surface.

As also illustrated in Figure 5, the intensity considerably decreases with the presence of the recombining surface. In this case the emission mostly originates from the afterglow present inside the quartz tube. The spectra, being dominated by the NO_γ and NO_β bands, suggests the presence of both N and O-atoms inside the quartz tube.

4.3. Characterization of the afterglow in the reactor

From the application point of view it is important to know the species densities and the temperature distributions in the reactor, as well as the influence of the treated tube's presence on these characteristics and on the flow dynamics.

The system characteristics are studied for the 1000 sccm N_2 - 20 sccm O_2 flow condition, when the surfatron is positioned at 7 cm from the reactor inlet, which at the 25 W input power results in a 2 cm long discharge and 5 cm long early-afterglow region. The discharge pressure depends on the pressure drop [31] occurring along the system at the different reactor loading conditions, as discussed in the following section.

4.3.1. Estimation of the pressure along the system The afterglow characteristics, besides the mixture composition and the system parameters are determined by the gas pressure. The pressure in the system, as illustrated in Figure 1, is measured at the gas inlet upstream of the discharge tube, and downstream of the reactor. In the

case of the empty reactor a pressure drop exists along the discharge tube due to its small diameter and the high gas flow rate used. When the gas flow rate is 1000 sccm this pressure drop is 16 mbar [31]. Assuming a linear dependence of the pressure drop on the tube's length, the pressure in the discharge and early-afterglow regions can be easily estimated. Meanwhile, the pressure in the reactor (late-afterglow) is equal to the pressure measured downstream [31].

When the reactor is loaded with the small diameter quartz tube and the afterglow is guided through it, a pressure gradient develops between the two ends of the treated tube, i.e. in the non-loaded part of the reactor the pressure increases considerably comparing to the empty reactor case. In order to measure the pressure in this region, the system set-up should be redesigned, which could further change the flow dynamics. However, the pressure here can be estimated by following the optical emissions spectra of species created in the afterglow through three-body reactions, i.e. species whose densities are directly influenced by the gas pressure. In the N_2-O_2 afterglow these are the NO(A) and NO(B) molecules created through the N + O + M $\rightarrow$ NO(A,B) + M processes [26].

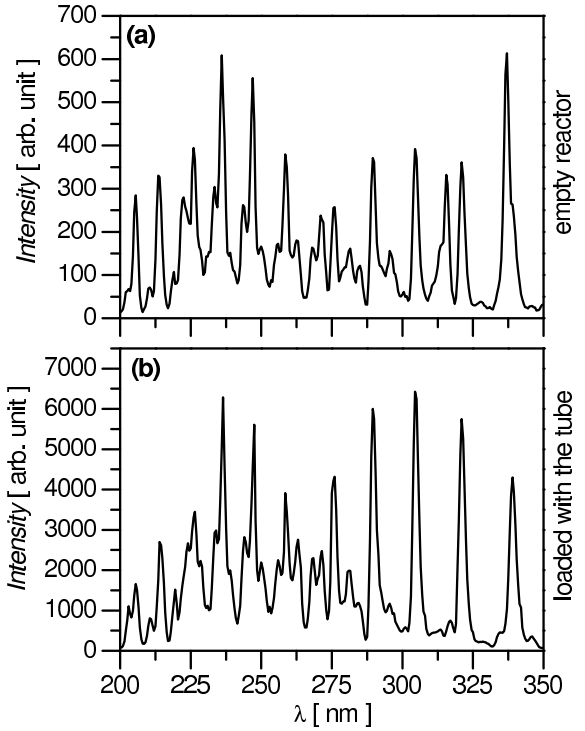

Figure 7. Spectra recorded in the reactor at 10 cm from the inlet (a) in the empty reactor and (b) in the reactor loaded with the tube. In the loaded reactor the afterglow is guided through the tube.

Figure 7 (a) and (b) show the spectra measured in the empty and the loaded reactor at 10 cm from the reactor's inlet. In both cases the pressure measured downstream of reactor, p_{end}, is 2 mbar. In the case of the loaded reactor - where the afterglow is guided through the tube - one order of magnitude higher intensity is achieved than in the empty

reactor. The one order of magnitude increase in the intensity suggests a considerable pressure increase. We also note, that in the loaded reactor the NO_β band - originating from NO(B) - becomes dominant over the NO_γ band of NO(A). The NO(A) molecules in the discharge are predominantly created through the $N_2(A) + NO \rightarrow N_2(X) + NO(A)$ reaction, which is still important in the early-afterglow (which can be still present in the reactor close to the inlet) until $N_2(A)$ is totally quenched. In the late-afterglow both NO(A) and NO(B) are exclusively created through the three-body re-association process.

In order to estimate the pressure in the loaded reactor, the here observed afterglow can be simulated in the empty reactor - where the pressure can be measured - by decreasing the pumping efficiency, and as a consequence to increase the pressure. This can be achieved by closing the valve towards the pumping system. Nevertheless, the density of radiating species besides the pressure is also influenced by the flow dynamics, which defines the density distributions. The flow dynamics of the loaded reactor can be simulated by placing a tube holder ring - which in this case is a 5 mm thick teflon ring with a 6.5 mm diameter central hole - into reactor while regulating the pressure. Although a pressure drop through the ring also occurs, the pressure measured downstream of the reactor can still give a close estimate of the pressure in front of the ring. The evolution of the species densities along the afterglow depends on the pressure and is well illustrated by the evolution of the emission originating from the excited species created in three-body reactions. The axial distribution of the intensity of one specific bandhead is measured along the system for the empty reactor, and for the reactor loaded with the tube and the ring, respectively, for different pressures, p_{end}, measured downstream the reactor.

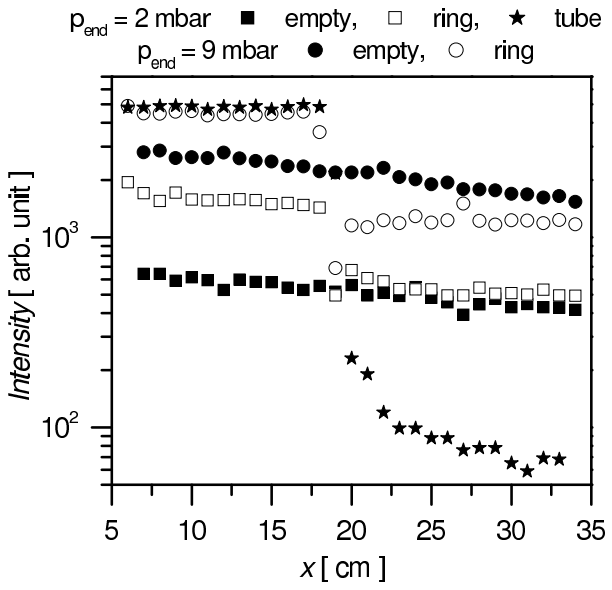

Figure 8. The axial distribution of the intensity at 236 nm measured in the empty and in the loaded reactor when the afterglow flows inside the tube at different pressures measured downstream the reactor.

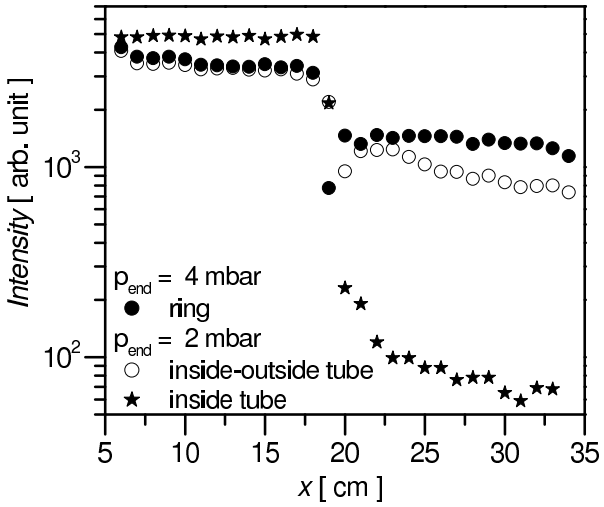

Figure 9. The axial distribution of the intensity at 236 nm measured in the reactor loaded with the tube holder ring, and with the tube when the afterglow flows inside and on both sides of the tube, respectively, at different pressures measured downstream the reactor.

Figure 8 shows the axial distribution of the intensity at 236 nm for the different reactor and pressure conditions. The presence of the tube holder ring in the reactor can be observed at around $x = 18.5$ cm. The results show that the intensity distribution measured in the reactor loaded with the quartz tube can be reproduced with the intensity distribution measured in the reactor with the presence of the ring when the pressure downstream of reactor is 9 mbar. On the other hand, in the reactor loaded with the tube holder ring slightly higher intensities are obtained than in the empty reactor for the same p_{end} pressures. This suggests that the pressure in front of the tube holder ring is higher than the one measured downstream the reactor. The intensity distribution also shows the effect of the flow on the distribution, while in the empty reactor the intensity decreases exponentially, in the loaded reactor, where the outlet is much smaller (5 mm and 6.5 mm versus 25 mm) and closer to the inlet (18 cm versus 40 cm), the intensity decrease is more moderate.

In the second case presented in Section 4.2, when the afterglow is guided both inside and around the quartz tube (which is held by a teflon ring with four pairs of 2 mm holes around the tube's position), the pressure increase in the non-loaded part of the reactor is more moderate. The axial distribution of the 236 nm bandhead's intensity, as shown in Figure 9, can be reproduced in the case of the reactor loaded with the ring alone at $p_{\text{end}} = 4$ mbar. The emission spectra measured in front of the ring for these two cases, presented in Figure 10, show a perfect fit for the whole spectra range covered by the NO_γ and NO_β emission.

For a better estimation of the pressure in the reactor and to get an insight into the species densities and temperature distributions in the reactor we can use the modelling technique. The comparison of the measured emission intensity and the calculated density distributions give the possibility to show the validity of the model (presented in

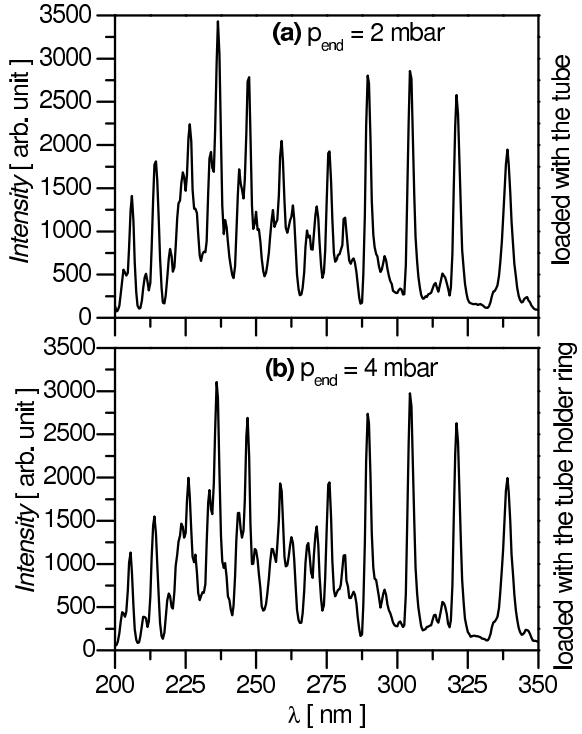

Figure 10. Spectra recorded at 10 cm from the reactor's inlet (a) in the reactor loaded with the tube, when the afterglow flows both inside and around the tube, and (b) in the reactor loaded with the tube holder ring. The spectra illustrate the pressure increase due to the presence of the tube.

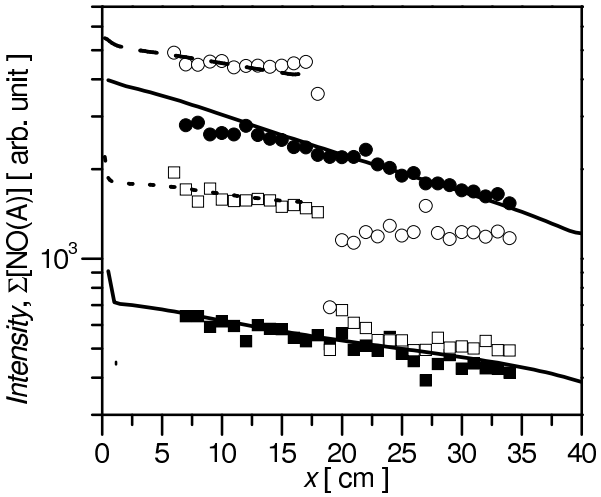

Figure 11. Measured intensity (symbols) and normalized calculated density (lines) distributions in the empty and in the reactor loaded with the ring at 2 mbar and 9 mbar downstream pressures. The symbols represent the same conditions as in Figure 8.

Section 3) [26], and afterwards, to estimate the pressure increase in the reactor in front of the treated tube. Under each afterglow condition the discharge and early-afterglow

conditions have been modified accordingly, by taking into account the change of the pressure drop along the discharge tube (The procedure and the effect of the pressure has been discussed in details in our previous publication [31]). Figure 11 shows the measured intensity and the calculated NO(A) density distributions for the empty reactor and for the reactor loaded with the tube holder ring at $p_{\text{end}} = 2$ mbar and 9 mbar conditions (We remind that, as shown in Figure 8, the same afterglow condition has been found in front of the ring in the reactor loaded only with the ring at $p_{\text{end}} = 9$ mbar and in the reactor loaded with the tube at $p_{\text{end}} = 2$ mbar.). In the case of the empty reactor, where the pressure in the reactor is equal with the pressure measured downstream, we find a very good agreement between the measured and calculated distributions. The calculated densities are normalized to the measured emission intensity distributions using the same normalization factor for both pressure cases. For the reactor loaded with the ring, we have found, that the measured intensity distributions can be reproduced by the calculated distributions when the pressure in front of the ring is chosen 3.5 mbar and 10.5 mbar instead of 2 mbar and 9 mbar, respectively. Here the same normalization factors are used as in the case of the empty reactor. Further on, Figure 12 shows the measured intensity and calculated NO(A) density distributions in front of the tube holder ring for the two type of tube treatment conditions. The measured and calculated distributions are in good agreement and indicate, that when the afterglow is guided through the tube the pressure in front of the tube in the reactor is about 11 mbar, while when the afterglow flows both inside and around the tube the pressure is 6.5 mbar. In both cases the pressure measured downstream the reactor is 2 mbar.

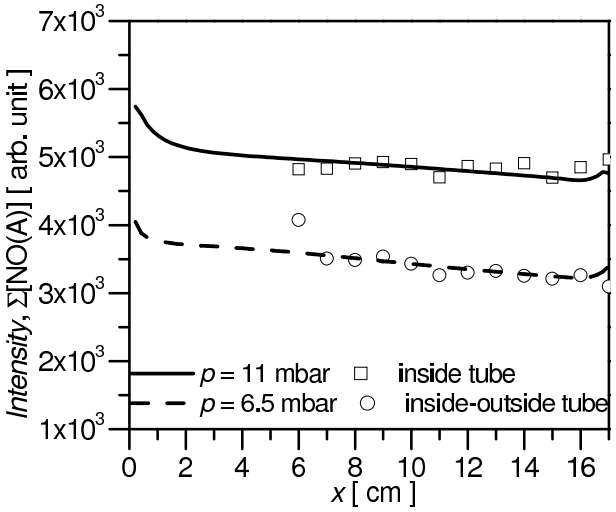

Figure 12. Measured intensity (symbols) and normalized calculated density (lines) distributions in the reactor loaded with the tube for the two type of treatments.

4.3.2. Temperature The reactor being filled with neutral late-afterglow the temperature measurement by thermocouple may be possible, as it does not influence

the discharge operation. Placing thermocouple in the reactor may influence the flow dynamics and minor decrease the atomic densities due to their recombination on the thermocouple surface, resulting in the increase of its temperature (similarly to the catalytic probes used for atomic density measurements [29, 52, 53]). Nevertheless, it can give a very good estimate of the gas temperature, as also demonstrated by our calculations.

We measured the temperature in the system with a thermocouple in three different cases. In the first case the thermocouple is positioned in the unloaded reactor on a teflon holder of 1 cm hight at 16 cm from the inlet. The temperature here is measured to be 323-328 K after 15 s the discharge has been turned on. Due to the recombination of species on the thermocouple the temperature rises and saturates at 343 K after 5 min. When the discharge is turned off the temperature rapidly falls, and when the temperature decrease slows down thermocouple shows the temperature of the teflon, which is found to be 323 K. In the second case the thermocouple is held at 2 cm height at 16.5 cm from the inlet with the help of a teflon ring, where the flow of the afterglow is allowed by eight symmetrically positioned 6 mm holes. Here the temperature is found to be 323 K at 20 W discharge power, 343 K at 25 W and 363 K at 30 W. In the last case the loaded reactor is simulated. In this case the reactor is loaded with the quartz tube held by the teflon rings with four pairs of 2 mm holes, allowing the flow of the afterglow both inside and around the tube, as discussed in Section 4.2. Here the thermocouple is fixed in one of the 2 mm holes at 2.8 cm height at 17 cm from the reactor inlet. Here the measured temperature is 323 K.

In the next step the temperature distribution in the reactor is determined with the 3-D hydrodynamic model for the different reactor conditions. The obtained distributions are presented in the middle vertical plane of the reactor - which is the symmetry plane - and shown in Figure 13. Figure 13 (a) and (b) present the temperature distribution in the empty reactor for 2 mbar and 9 mbar pressures, showing that with pressure the temperature does not change significantly in the reactor. The calculated temperatures show very good agreement with the measured temperatures presented in the previous paragraph.

During the present studies the tube has been placed in the reactor at the $x = 17$ cm position. According to the calculated temperature distributions, the gas temperature at the tube inlet is about 342 K. The temperature distributions in the loaded reactors in front of the tube holder ring are shown in Figure 13 (c) and (d). Although the distributions slightly change due to the different size and position of the outlet, in the central axis of the reactor, where the tube is positioned, similar temperatures are obtained as in the case of the empty reactor. Nevertheless, the increase of the temperature can be expected from the recombination of the atoms on the tube holder ring. The heating of the tube holder ring by surface recombination processes becomes more important with increasing the pressure, i.e. of the absolute density of species, as well as with the treatment time. Therefore it is very important to choose materials with low surface recombination probabilities.

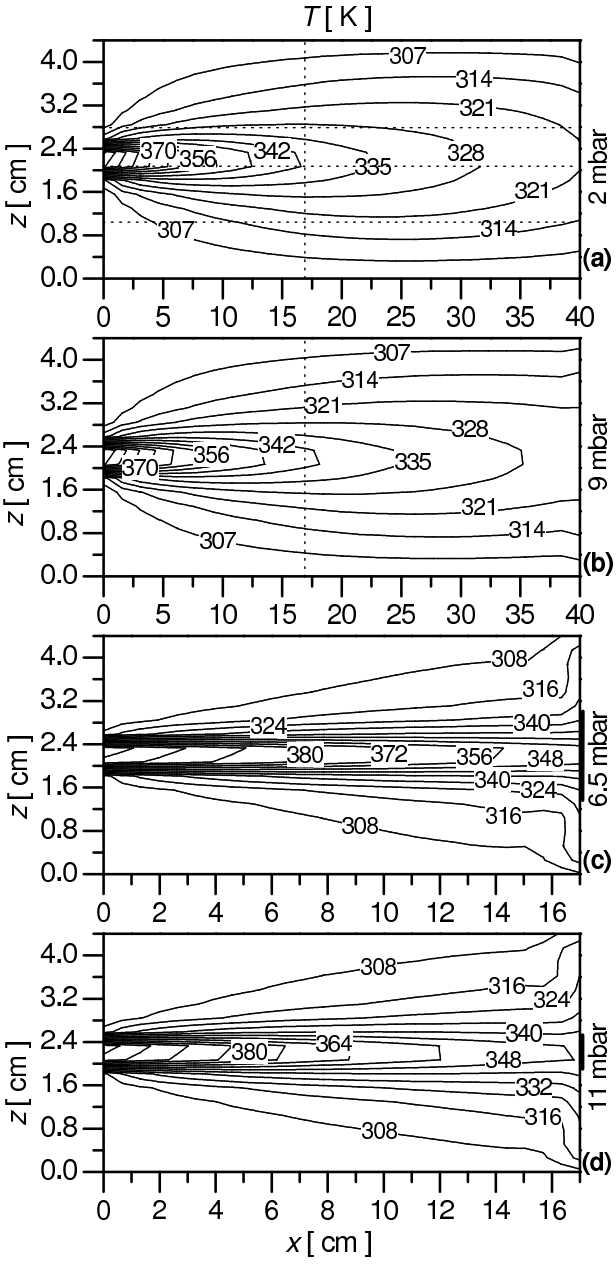

Figure 13. The temperature distribution in the middle vertical plane of the reactor in the case of empty (a)-(b) and loaded (c)-(d) reactors.

4.3.3. Active species In the reactor the density distribution of species are calculated for the empty reactor case and for the loaded reactor case in front of the tube holder ring, in order to follow the changes in the density distributions due to the load and as a consequence, of the pressure increase. Figure 14 and Figure 15 show the density distributions of the oxygen and nitrogen atoms, respectively. Due to the pressure increase, in the case of both atomic species a considerable density increase can be observed when the reactor is loaded. However, for the same reason - i.e. due to the enhanced three body gas phase recombination - the relative densities decrease, more

pronounced in the case of N-atoms from 5.3×10^{-3} to 3.4×10^{-3}. On the other hand, in the case of the O_2(a) molecules both the relative and absolute densities increase, as shown in Figure 16. Furthermore, the density distribution of O_2(a) is close to homogeneous, slight increase in absolute density along the reactor is observed due to the temperature decrease.

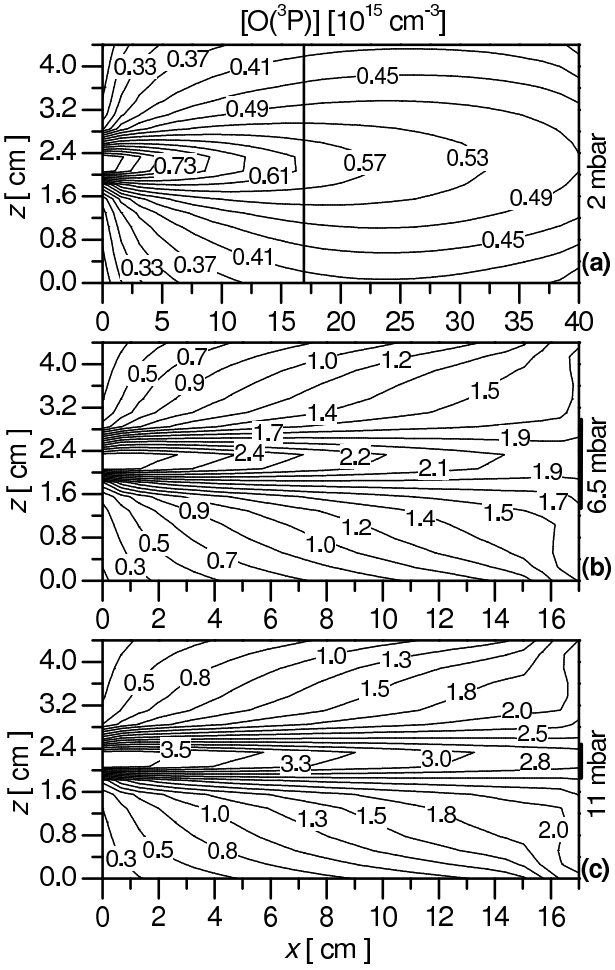

Figure 14. Density distribution of O-atoms (a) in the empty reactor, and in the loaded reactor in front of the tube holder ring when (b) the afterglow flows both inside and around the small diameter tube, and (c) the afterglow is guided through the tube. The distributions are shown in the vertical symmetry plane.

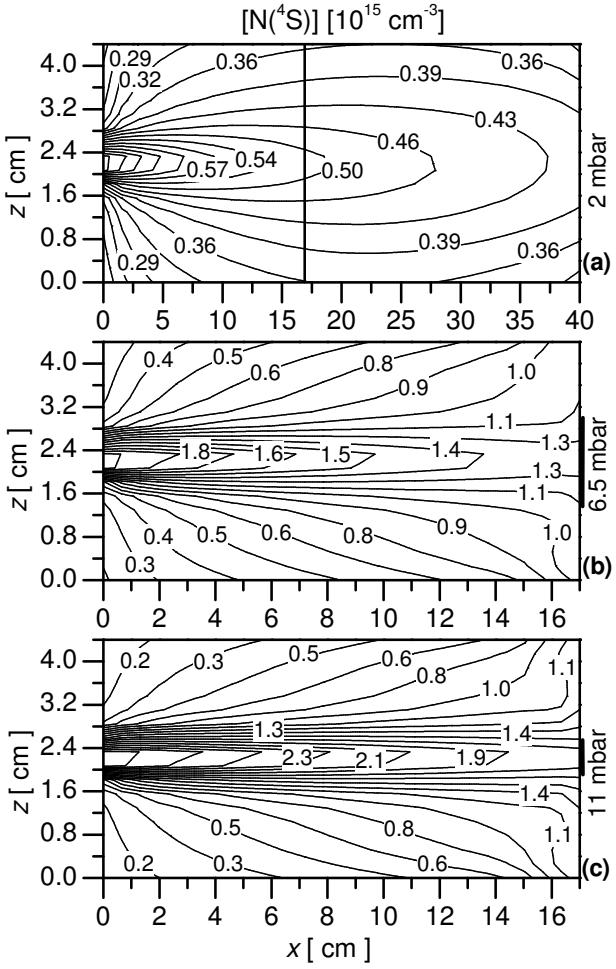

Figure 15. Density distribution of N-atoms in the reactor for the same conditions as in Figure 14.

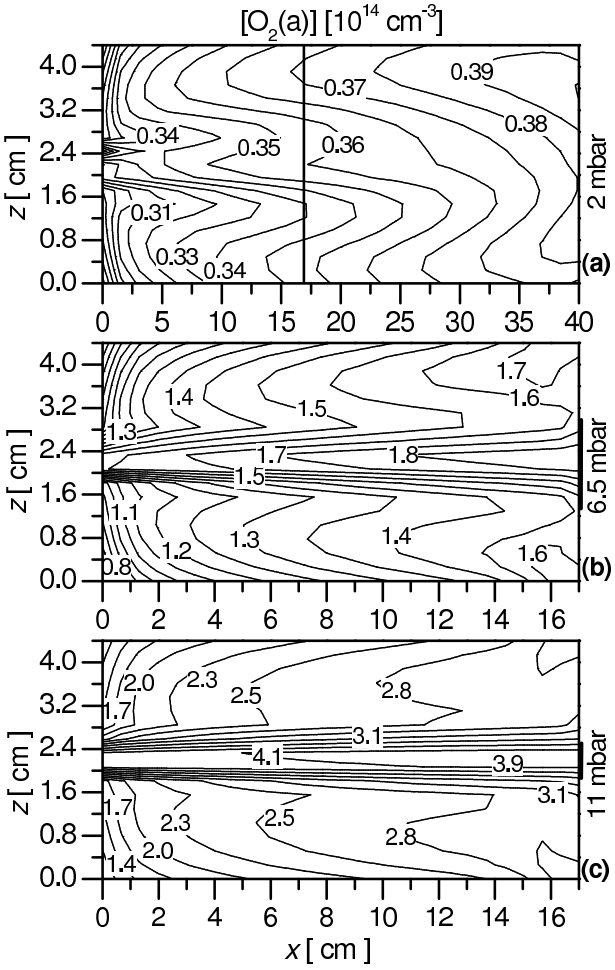

Figure 16. Density distribution of O_2(a) molecules in the reactor for the same conditions as in Figure 14.

4.4. Afterglow inside the small diameter tube

In order to follow the evolution of the afterglow inside the 5 mm diameter quartz tube, the axial distribution of the UV radiation has been measured, as presented in Section 4.1. Furthermore, an attempt has been made to access also the density distribution of species in the tube, by calculating the evolution of the afterglow as flows through the tube. The difficulty is given by the pressure drop occurring along the tube. As a first approximation calculations have been conducted for the medium pressure, and the change of pressure along the tube has been taken into account only in the chemical kinetic scheme. Figure 17 shows the comparison of the measured intensity and the calculated NO(A) density distributions. As shown by the figure, assuming a linear pressure drop along the tube, the measured distribution could not be reproduced. The axial distribution of the emission resulting from the NO(A) molecules created through the three-body reaction, and as such reflecting the evolution of the pressure, suggest a second order pressure drop along the tube. The density distribution calculated assuming a second order pressure

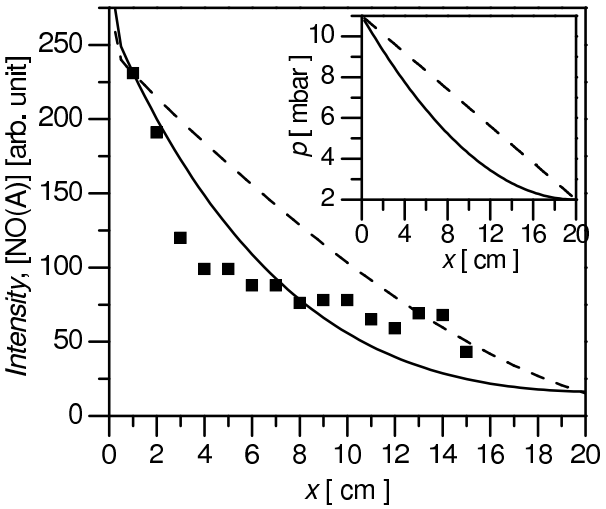

Figure 17. Measured intensity (symbols) and normalized calculated density (lines) distributions along the 5 mm diameter quartz tube, when the afterglow is guided through it. The broken and full lines show the density distributions when the pressure drop along the tube is assumed to be linear and second order, respectively, as illustrated in the inserted panel.

drop, as illustrated in the inserted panel of Figure 17, reproduces well the measured distribution. Afterwards, using this condition the density distributions of active species along the tube are also calculated.

Figure 18 (a) shows the relative density of NO(A) in the symmetry plane of the 0.5 mm tube, when the afterglow is guided through it. The relative density of NO(A) decreases one order of magnitude along the tube, while the pressure decreases from 11 mbar to 2 mbar. Meanwhile, the relative densities of atomic species, whose kinetics are not governed by three-body reactions, do not decrease considerably. Furthermore, the relative density of O_2(a) molecules stays constant along the tube. These results show, that the absolute density of active species along the tube decrease mostly due to the pressure (i.e. total density) drop, while the UV emission decreases due to the lower sources of NO(A) and NO(B) molecules from the three-body reactions.

5. Conclusions

In the present study we have investigated the possibility of treating the surfaces of heat sensitive small diameter tubes in the flowing afterglow of a low pressure surface-wave microwave discharge, using an N_2-O_2 mixture discharge. We have demonstrated, that the afterglow can be efficiently guided through a 4.5 mm inner diameter tube, as well as, the inner and outer wall surfaces can be simultaneously treated.

We have followed the evolution of the afterglow in the reactor and in a 5 mm ID quartz tube placed into reactor through the optical emission, namely the UV radiation originating from the excited NO molecules, and demonstrated that the emission spectra

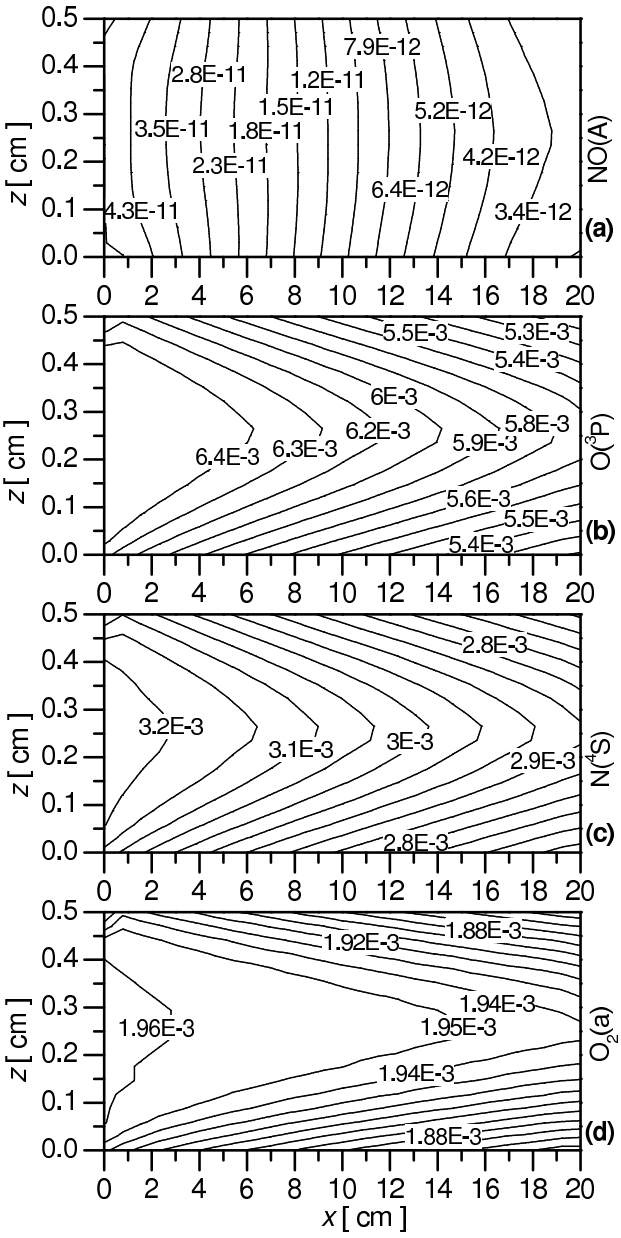

Figure 18. Species density distributions in the vertical symmetry plane of the 5 mm diameter tube, when the afterglow is guided through it.

can serve as a good diagnostic for the estimation of the pressure in the system and to prove the presence of the N and O-atoms. The measured axial distribution of the emission intensity served also to show the validity of the 3-D hydrodynamic model used to calculate the afterglow characteristics, both in the reactor and inside the small diameter tube.

We have shown that the pressure in the reactor increases considerably when it is loaded with a small diameter tube. This results the increase of the density of active species: N and O-atoms, and O_2(a) molecules in the non-loaded part of the reactor,

which further enter the tube placed into reactor. On the other hand, as a consequence of the pressure drop developed along this tube, the UV emission strongly decreases along it, which is the result of the decreasing sources of the excited molecules from the three-body processes. Meanwhile the absolute density of active species decrease mostly due to the pressure (density) drop, since their relative density do not change considerably along the tube. Therefore, in this region the UV emission is not a good indicator for the behaviour of the atomic densities.

Keeping in mind the requirements for the treatment of heat sensitive tubes, we have measured the temperature in the reactor at chosen locations and also calculated its distribution. We have shown that the temperature does not change considerably with the load, however its positioning should be carefully chosen. In the present reactor, that is a 4.4 cm diameter 40 cm long tube, the heat sensitive samples should be placed in the second half of the reactor. Furthermore, the tube holder should be made from a material with a low surface recombination probability, as its temperature can increase due to the surface recombination processes, more significantly at higher pressures and treatment times.

From the application point of view, we note that the system would also allow the simultaneous treatment of several tubes at different gas mixtures (e.g. non UV emitting Ar-O_2 afterglow).

Acknowledgments

The work has been supported by Hungarian Science Foundation NKFIH through K-104531.

References

[1] Moisan M, Boudam K, Carignan D, Keroack D, Levif P, Barbeau J, Seguin J, Kutasi K, Elmoualij B, Thellin O, Zorzi W 2013 *Eur. Phys. J. Appl. Phys.* **63** 10001
[2] Villeger S, Cousty S, Ricard A and Sixou M 2003 *J. Phys. D: Appl. Phys.* **36** L60
[3] Raballand V, Benedikt J, Wunderlich J and von Keudell A 2008 *J. Phys. D: Appl. Phys.* **41** 115207
[4] Cvelbar U, Mozetič M, Hauptman N and Klanjšek-Gunde M 2009 *J. Appl. Phys.* **106** 103303
[5] Rossi F, Kylián O, Rauscher H, Hasiwa M and Gilliland D 2009 *New J. Phys.* **11** 115017
[6] Rauscher H, Kylián O, Benedikt J, von Keudell A and Rossi F 2010 *ChemPhysChem* **11** 1382
[7] Vesel A, Kolar M, Recek N, Kutasi K, Stana-Kleinschek K, Mozetic M 2014 *Plasma Process. Polym.* **11** 12
[8] Balazs D J, Triandafillu K, Wood P, Chevolot Y, van Delden C, Harms H, Hollenstein C and Mathieu H J 2004 *Biomaterials* **25** 2139
[9] Belmonte T, Pintassilgo C, Czerwiec T, Henrion G, Hody V, Thiebaut J and Loureiro J 2005 *Surf. Coat. Technol.* **200** 26
[10] Amanatides E, Mataras D, Katsikogianni M and Missirlis Y 2006 *Surf. Coat. Technol.* **200** 6331
[11] Krstulović N, Labazan I, Milošević S, Cvelbar U, Vesel A and Mozetič M 2006 *J. Phys. D: Appl. Phys.* **39** 3799
[12] Cvelbar U, Pejovnik S, Mozetič M and Zalar A 2003 *Appl. Surf. Sci.* **210** 255
[13] Mafra M, Belmonte T, Poncin-Epaillard F, Maliska A and Cvelbar U 2009 *Plasma Process. Polym.* **6** S198

[14] Vesel A, Kolar M, Doliska A, Stana-Kleinschek K, Mozetic M 2012 *Surf. Interface Anal.* **44** 1565
[15] Mozetič M, Primc G, Vesel A, Zaplotnik R, Modic M, Junkar I, Recek N, Klanjšek-Gunde M, GuhyL , Sunkara MK , Assensio M C, Milošević S, Lehocky M, Sedlarik V, Gorjanc M, Kutasi K, Stana-Kleinschek K 2015 *Plasma Sources Sci. Technol.* **24** 015026
[16] Kolar M and Primc G 2016 *Int. J. Polym. Sci.* 1749285
[17] Afonso Ferreira J, Nguyen H P T, Mi Z, Leonelli R and Stafford L 2014 *Nanotechnology* **25** 435606
[18] Prégent J, Vandsburger L, Blanchard V, Blanchet P, Riedl B, Sarkissian A, Stafford L 2015 *Cellulose* **22** 811
[19] Tóth A, Szentmihályi K, Keresztes Zs, Szigyártó I, Kováčik D, Černák M, K Kutasi K 2015 *Open Chemistry* **13** 557
[20] Kidane A G, Salacinski H, Tiwari A, Bruckdorfer K R, Seifalian A M 2004 *Biomacromolecules* **5** 798
[21] Cheruthazhekatt S, Černák M, Slavíček P, Havel J 2010 *J. Appl. Biomed.* **8** 55
[22] Ding X, Yang Ch, Lim T P, Hsu L Y, Engler A C, Hedrick J L, Yang Y-Y 2012 *Biomaterials* **33** 6593
[23] Rezaei F, Abbasi-Firouzjah M, Shokri B 2014 *J. Phys. D: Appl. Phys.* **47** 085401
[24] Duday D, Clément F , Lecoq E , Penny C , Audinot J-N , Belmonte T , Kutasi K , Cauchie H-M , Choquet P 2013 *Plasma Process. Polym.* **10** 864
[25] Canal C, Gaboriau F, Ricard A, Mozetic M, Cvelbar U and Drenik A 2007 *Plasma Chem. Plasma Process.* **27** 404
[26] Kutasi K , Saoudi B, Pintassilgo C D, Loureiro J, Moisan M 2008 *Plasma Process. Polym.* **5** 840
[27] Ricard A, Moisan M, Moreau S 2001 *J. Phys. D: Appl. Phys.* **34** 1203
[28] Kutasi K, Guerra V, Sá P A 2011 *Plasma Sources Sci. Technol.* **20** 035006
[29] Kutasi K , Zaplotnik R , Primc G , Mozetic M 2014 *J. Phys. D: Appl. Phys.* **47** 025203
[30] Afonso Ferreira J, Stafford L, Leonelli R and Ricard A 2014 *J. Appl. Phys.* **115** 163303
[31] Kutasi K, Noel C, Belmonte T and Guerra V 2016 *Plasma Sources Sci. Technol.* **25** 055014
[32] Hatada K, Miyajima O, Kobayashi H 1984 U.S. Patent Number 4488954
[33] Narayanan P V 1995 *J. Biomaterials Science* **6** 181
[34] Khoo K, Takeuchi M, Onuki J and Urao R 2004 *Materials Transactions* **45** 599
[35] Lauer J L, Shohet J L, Albrecht R M, Esnault S, Malter J S, von Andrian U H and Shohet S B 2005 *IEEE Trans. Plasma Sci.* **33** 791
[36] Cao L, Ratner B D, Horbett T A 2007 *J. Biomed. Mater. Res. A* **81A** 12
[37] Kovalova Z, Leroy M, Jacobs C, Kirkpatrick M J, Machala Z, Lopes F, Laux C O, DuBow M S and Odic E 2015 *J. Phys. D: Appl. Phys.* **48** 464003
[38] Pollak J, Moisan M, Kéroack D, Séguin J and Barbeau J 2008 *Plasma Process. Polym.* **5** 14
[39] Xiong Z, Robert E, Sarron V, Pouvesle J-M and Kushner M J 2013 *J. Phys. D: Appl. Phys.* **46** 155203
[40] Chen F, Song J, Huang S, Xu S, Xia G, Yang D, Xu W, Sun J and Liu X 2016 *J. Phys. D: Appl. Phys.* **49** 365202
[41] Boudam M K, Saoudi B, Moisan M and Ricard A 2007 *J. Phys. D: Appl. Phys.* **40** 40 1694
[42] Pointu A-M, Ricard A, Odic E, Ganciu M 2008 *Plasma Process. Polym.* **5** 559
[43] Junkar I, Cvelbar U, Vesel A, Hauptman N, Mozetic M 2009 *Plasma Process. Polym.* **6** 667
[44] Boudam M K, Moisan M, Saoudi B, Popovici C, Gherardi N, Massines F 2006 *J. Phys. D: Appl. Phys.* **39** 3494
[45] Kutasi K, Guerra V and Sá P 2010 *J. Phys. D: Appl. Phys.* **43** 175201
[46] Guerra V, Kutasi K, Sá P A, Lino da Silva M 2011 *Eur. Phys. J. Appl. Phys.* 56 24004-p1
[47] Pintassilgo C D, Loureiro J, Guerra V 2005 *J. Phys. D: Appl. Phys.* **38** 417
[48] Kutasi K, Pintassilgo C D and Loureiro J 2009 *J. Phys.: Conf. Series* **162** 012008
[49] Guerra V, Loureiro J 1999 *Plasma Sources Sci. Technol.* **8** 110
[50] Kutasi K, Pintassilgo C D, Coelho P J, Loureiro J 2006 *J. Phys. D: Appl. Phys.* **39** 3978
[51] Kutasi K and Loureiro J 2007 *J. Phys. D: Appl. Phys.* **40** 5612

[52] Mozetic M, Cvelbar U, Vesel A, Ricard A, Babic D and Poberaj I 2005 *J. App. Phys.* **97** 103308
[53] Drenik A, Cvelbar U, Ostrikov K and Mozetic M 2008 *J. Phys. D: Appl. Phys.* **41** 115201